SAFETY EVALUATIONS ON UNIGNITED HIGH-PRESSURE METHANE JETS IMPACTING A SPHERICAL OBSTACLE

Cristian Colombini, Edoardo Carminati, Andrea Parisi, Renato Rota, Valentina Busini *

Politecnico di Milano - Department of Chemistry, Materials and Chemical Engineering "Giulio Natta", Piazza Leonardo da Vinci 32, 20133, Milano, Italy

* Corresponding author:

E-mail address: valentina.busini@polimi.it

ABSTRACT

Nowadays methane is a fossil fuel widely used both in industries and in civil appliances. From the safety point of view, due to its flammability, its use implies hazards for people and assets. The hazardous area related to a high-pressure jet of methane arising from an accidental loss of containment requires the estimation of the distance at which the methane concentration falls below the Lower Flammability limit. Such a topic is well covered in the literature when considering free jet conditions, *i.e.*, jets that do not interact with any equipment or surface. The same cannot be said for high pressure jets impacting an obstacle. In this context, the present work focuses on studying high pressure methane jets impacting spherical obstacles by means of Computational Fluid Dynamics with the aim of giving some insights about such a jet-obstacle interaction, possibly providing a brief by-hand procedure that, only based on known scenario information, allows to estimate the maximum extent of the unignited high-pressure jet when interacting with a spherical obstacle.

KEYWORDS

High-pressure release; methane; spherical obstacle influence; risk assessment; CFD; analytical correlation

ACRONYMS

CFD Computational fluid Dynamics

EDM Equivalent Diameter Model

FF Flash Fire

EoS Equation of State

HP High-Pressure

LFL Lower Flammability Limit

ME Maximum Extent

O&G Oil and Gas

RANS Reynolds Averaged Navier-Stokes

NOMENCLATURE

A_{ps}: pseudo-source area extension

c: methane concentration in air

c_{ax}: methane concentration along the free jet axis

C_D: discharge coefficient

C_p: methane heat capacity

d: actual orifice diameter

D: distance of the centre of the spherical obstacle from the jet source

d_{FJ}: free jet diameter

D_L: obstacle legs diameter

D_{NT}: obstacle distance from the jet source

d_{ps}: pseudo-source orifice diameter

D_T: obstacle diameter

H: jet source height

k: axial decay constant

$\dot{m}_{ps}$: pseudo-source mass flow rate

ME: jet axial maximum extent

ME_{FJ}: free jet LFL cloud maximum extent in direction of the jet axis

N_L: number of obstacle legs

p: upstream methane pressure

p_{amb}: environmental pressure

p_{ps}: methane pressure at pseudo-sourceconditions

T: upstream methane temperature

T_{ps}: methane static temperature at pseudo-source conditions

v_{ps}: methane velocity at pseudo-source conditions

α: angle between vertical direction and the points in proximity of the obstacle surface where velocity is recorded

γ: specific heat ratio

ρ_{ps}: methane density at pseudo-source conditions

ρ_{amb}: air density

1. INTRODUCTION

Methane is a clean and efficient hydrocarbon largely used in industry, commercial and residential sectors as well as for vehicles power (Sun, 2019; Varsegova et al., 2019; Zhu et al., 2020). Together with hydrogen, methane is expected to play a relevant role in the energy sector in the future (Zhou et al., 2018; Zhang et al., 2020). It can be handled, shipped and stored in liquefied form, keeping the fluid at very low temperatures (Zhang et al., 2020) or in gaseous form (Jafari et al., 2014) at pressures much higher than the ambient one.

In the second case, which is widely common to have, one of the safety related issues is the accidental release from a High-Pressure (HP) vessel or pipeline (Zhu et al., 2013). Considering the flammable nature of the methane jet, studies on its release characteristics and flow behavior are crucial for the risk assessment and management. This because if late ignition of the release occurs, the established Flash Fire (FF) can dramatically lead to a series of subsequent large scale events threatening people inside and even outside plant boundaries. Thus, the hazardous distance estimation, which is commonly evaluated as the distance where the flammable gas concentration

falls below either the Lower Flammability Limit (LFL) or LFL/2, becomes a crucial information to be predicted (Souza et al., 2019b). It is, therefore, quite evident the importance of predictive computational methods by which it is possible to assess the magnitude of the unignited accidental release (Rian et al., 2016).

It should be remarked that, thinking to an industrial accidental scenario in which a leak of methane from high-pressure conditions occurs, the situation of a congested area or, more in general, of a geometrically complex environment in which the leak can be placed (*e.g.*, in the vicinity of an obstacle), it might be considered. As widely reported in literature, the analytical correlations (c.f., Becker et al., 1967; Thring and Newby, 1952; Chen and Rodi, 1980) and the integral models (c.f., DEGADIS, SLAB, ALOHA, and UDM; Brook et al., 2003; Bernatik and Libisova, 2004; EPA, 2011; Pandya et al., 2012) developed within the industrial safety framework are reliable when analyzing a free jet scenario (intended as a release occurring in an unconfined environment, Dey et al., 2017), showing they limits when dealing with a situation in which a HP jet interacts with an obstacle (Cameron and Raman, 2005; Derudi et al., 2014; Pontiggia et al., 2014; Schelder et al., 2015; Gerbec et al., 2017; Uggenti et al., 2017; Dasgotra et al., 2018). Computational Fluid Dynamics (CFD) is the numerical approach traditionally employed to face such industrial safety issue (Deng et al., 2018; Souza et al., 2019a; Tolias et al., 2019) since it allows to address for any geometrical complexity (Efthimiou et al., 2017; Gerbec et al., 2017; Luo et al., 2018; Jiang et al., 2020).

Consequently, previous literature about unignited HP jets impacting an obstacle studied with the CFD is available, as summarized in the following. Benard et al. (2007) investigated the influence of flat surfaces parallel to unignited hydrogen and methane high-pressure jets. Tchouvelev et al. (2007) combined the commercial CFD software PHOENICS with two analytical models to investigate HP unignited hydrogen releases impinging against a protective wall. Desilets et al. (2009) performed an experimental campaign aiming to characterize the shape of the plume of different unignited hydrogen jets when influenced by a nearby horizontal flat surface. For comparison purposes, CFD numerical simulations have been also carried out. Hourri et al. (2009) extended the analysis of Benard et al. (2007) adding two distances of the jet source from the surface. Benard et al. (2009) further extended the previous analyses by considering more orifice diameters, storage pressures and distances from the flat surface. Houf et al. (2010) conducted a numerical evaluation of barrier walls for the mitigation of hydrogen releases, both ignited and unignited. Middha et al. (2010) performed a small scale experimental campaign on ignited HP

hydrogen jets interacting with an obstacle with the purpose of validating the commercial CFD software FLACS for this specific scenario. Hourri et al. (2011) and Angers et al. (2011) further extended the analysis of Hourri et al. (2009) considering several higher pressures and a different jet orientation, respectively. Pontiggia et al. (2014) compared the results of an integral model (PHAST) to the ones of a CFD model (FLUENT) for the case of an unignited HP methane jet impacting a cylindrical obstacle showing that, in this scenario, integral models become unreliable. Using the CFD code FLACS, Benard et al. (2016) investigated how a vertically or horizontally oriented flat surface influences the maximum extent of the lower flammability limit cloud of both hydrogen and methane unignited HP jets. They also derived engineering correlations able to substitute the use of more computationally expensive CFD software. Gerbec et al. (2017) analyzed the case of a vertical unignited propane jet impacting against the roof of a refueling station, comparing the results computed with a CFD software (FLUENT) and an integral model (UDM). They showed differences in predicting the damage area extension when using the two kinds of model. Of the same year it is the work of Hall et al. (2017), where they investigated how two horizontal surfaces (namely, the ground and the ceiling) influence unignited HP hydrogen clouds at different concentrations. Starting from the state of the art regarding CFD modeling for risk assessment of offshore installations, Uggenti et al. (2017) proposed a new hybrid approach, combining a semi-empirical model with a CFD one. Hu et al. (2018) accounted for the problem of unignited HP hydrogen jets impacting a vertical obstacle with the novelty of using a specific equation of state (EoS) (*e.g.*, Abel-Noble (Johnston, 2005)) to model gas density. Colombini and Busini (2019a and 2019b) studied the impingement of an unignited high-pressure methane jet on a cylindrical obstacle, both horizontally and vertically oriented. The focus has been on evaluating how a realistic obstacle influences the jet behavior, as function of the geometrical parameters of the scenario. Colombini et al. (2020a and 2020b) extensively investigated the effect of the ground on an unignited high-pressure jet of methane, hydrogen, and propane. Targeting to obtain simple relationships for risk assessment, Colombini et al. (2020c) performed an extensive CFD analysis of a realistic accidental scenario involving a high-pressure unignited methane jet impacting a pipe rack.

Despite, on one hand, the extensive use of the CFD in the framework of risk assessment research and, on the other one, the technological improvements of the computing resources, the CFD is not drawbacks-free: computational costs and analyst skills required are still a limitation on its use (Zuliani et al., 2016; Jiang et al., 2020). Therefore, the availability of quick and simple engineering

correlations allowing the estimation of the damage area of unignited impinging accidental releases might be useful.

Based on the depicted capabilities, the idea is that an extensive one-time-use of the CFD can be exploited as database-maker from which deriving simpler analytical relationships (Jiang et al., 2020) therefore avoiding the huge costs related to a full scale experimental approach (Wilkening and Baraldi, 2007).

In this context, the present work provides quick tools for daily activities in the risk assessment field. Considering as realistic accidental situation the case of an unignited high-pressure methane jet impacting a spherical obstacle (common for the storage of pressurized gasses, e.g. Liquefied Petroleum Gas), varying the distance between the release source and the obstacle as well as obstacle diameter, storage pressure and concentration level observed, we investigated several possible configurations of this scenario. From such configurations, we derived two instruments allowing to predict: i) when the obstacle influence expires (thus allowing the use of well-established analytical correlations for the modeling of the free jet case) and, ii) when present, how, by order of magnitude, the obstacle influence can be predicted.

2. METHODOLOGY

The scenario analyzed in this work is a horizontal high-pressure methane jet impinging a spherical obstacle. To study the influence of the obstacle on the jet development, several parameters (both of jet source and obstacle) were varied: upstream methane pressure (p); obstacle diameter (D_T); distance between jet source and obstacle (D_{NT}). The methane source was modelled as generated from a nozzle located in correspondence of the mid-height of the sphere (H): in all the analysis, it was kept constant and equal to 10 m in order to avoid any influence of the ground, therefore allowing to investigate the effect of the spherical obstacle alone. Note that the effect of the ground has been already discussed in detail in a previous work (Colombini et al., 2020a). Figure 1 shows a sketch of the scenario, where the relevant geometric characteristics are also defined. Different methane concentration values in air were considered apart from 5.3%, that is the methane LFL. A constant wind of 5 m/s blowing alongside and in the same direction of the jet was considered. On the overall, 264 different conditions were investigated, as summarized in Table 1S of the Supplementary Information.

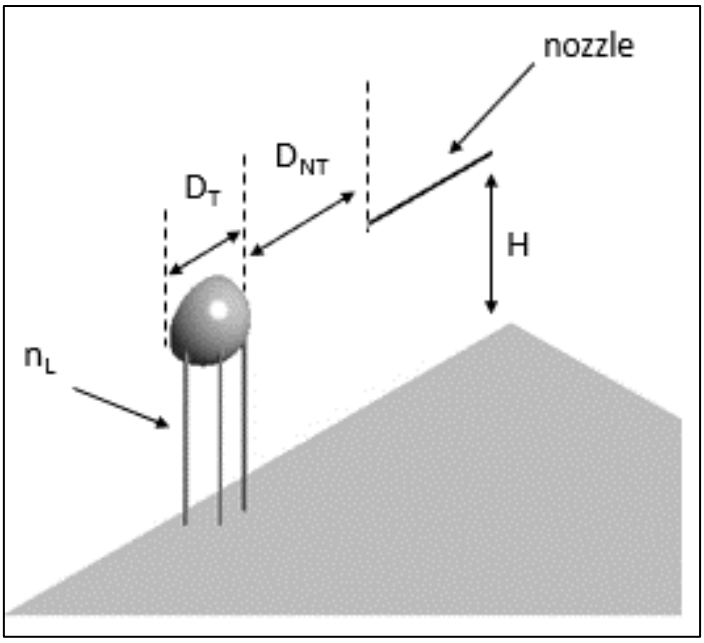

Fig. 1: Sketch of the basic scenario, symmetric with respect to the vertical plane crossing the jet axis, where are indicated key geometrical parameters of the scenario.

To build the CFD-computed information dataset, the commercial package Ansys Workbench v. 19.1 was used (Ansys Workbench, 2017). In particular, DesignModeler, Meshing and Fluent were the software by which realization of the computational fluid domain, fluid volume division in cells and resolution of the fluid governing equations was performed, respectively (Ansys DesignModeler User Guide, 2017; Ansys Meshing User Guide, 2017; Ansys Fluent User Guide, 2017).

Due to a large pressure difference between the vessel/pipeline and the environment as in all the cases analyzed in this work, a supersonic jet is expected, leading to a high demand of computational resources (Colombini et al., 2020a). However, since the focus of the work is on the so-called farfield zone of the jet (*i.e.*, far from the jet source), the commonly adopted way of using empirical relationships to model the supersonic release source through the approach referred to as the Equivalent Diameter Model (EDM) has been used (Hess et al., 1973; Sposato et al., 2003; Pontiggia et al., 2014; Benard et al., 2007; Houf et al., 2007; Stewart et al., 2019; Tolias et al., 2019; Franquet et al., 2015). In particular, the model developed by Birch et al. (1984) has been used for all the computations carried out, whose equations are summarized in Table 1. The computational domain extents were sized following the strategy described in the work of Colombini et al. (Colombini et al., 2020c) leading to a rectangular box of 120 m length, 25 m height

and 15 m wide was used. Note that 15 m is half the width of the domain, thanks to the symmetry of the geometry. The strategy used for the domain discretization is discussed in detail elsewhere (Colombini et al., 2020a). In this way an optimized grid was obtained, with a finer mesh surrounding the jet axis (which is the computationally critical zone), and a less dense one close to the domain boundaries (where demanding physical phenomena are not expected). The *inflation* mesh feature was used for a specific grid definition of the cells surrounding the obstacle surface (Ansys Meshing User Guide, 2017). The grid obtained was tetrahedral, fully unstructured; taking run 11_M in Table 1S as example, Figure 2 shows how the resulting domain discretization appears. Depending on the specific case considered, which is related to the values of the involved parameters, the number of cells ranged from 3.5 to 8 million. Quality requirements in terms of skewness and orthogonal quality were always satisfied. Considering run 11_M in Table 1S as benchmark case, the grid independence of the results is summarized in Figure 1S in the Supplemental Information, which shows the comparison of the sensitivity analysis results in terms of cloud maximum axial extent (ME) variations with respect to different mesh refinements.

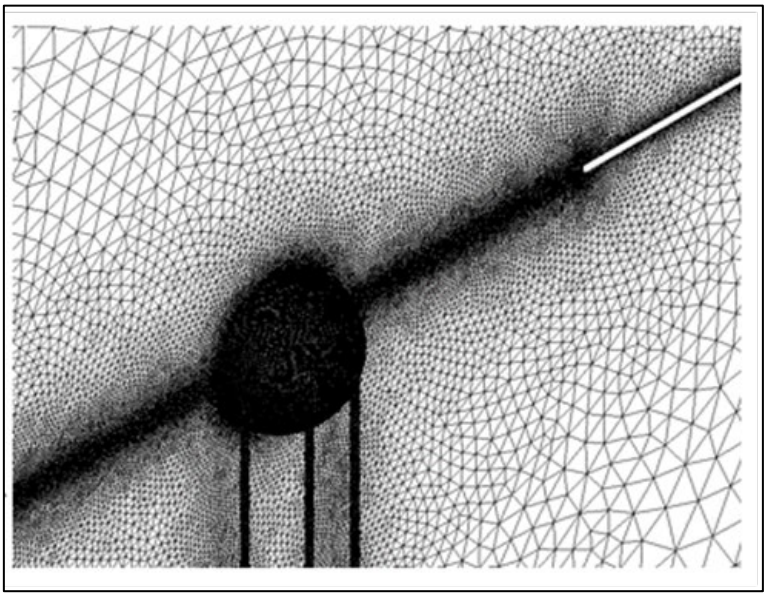

Fig. 2: Surface grid for run $11_{M,}$ highlighting the large cells density in correspondence of the jet axis and the obstacle surface obtained thanks to the mesh features deployed.

For what concerns numerical settings, the Reynolds-averaged approach was employed for the governing Navier-Stokes equations (RANS approach) coupled with the two-equation eddy-viscosity k-ω SST turbulence closure model (Menter, 1993). All the simulations were performed in steady state conditions and the pressure-based solver was chosen thanks to the EDM approach, which allows the flow to be treated as incompressible. To account for the multi-species problem

(methane release in ambient air), the species transport model was selected and the ideal gas EoS was used to model the fluid mixture density. The COUPLED pressure-velocity coupling scheme was adopted, while the second order upwind spatial-discretisation scheme was considered for all the convective terms. Table 2S in the Supplemental Information lists the model equations together with the definition of the main parameters. Gravity acceleration was always included perpendicularly to the ground surface. Table 1 summarizes the equations defining the methane inlet boundary condition (based on the EDM model of Birch et al., 1984), while Table 2 reports the other boundary conditions used. Finally, to give an overview on the methodological steps that were followed, Figure 3 shows the numerical methodology flow chart.

Table 1: EDM equations from the Birch et al. (1984) model defining the pseudo-source of the methane jet. In the Equations, d_{ps} is the resulting diameter of the pseudo-source, d is the actual orifice diameter, C_D is the discharge coefficient, p is the storage pressure, p_{amb} is the environmental pressure, γ is the specific heat ratio, Cp is the methane heat capacity, $\dot{m}_{ps}$, v_{ps}, ρ_{ps}, T_{ps}, p_{ps} and A_{ps} are the resulting mass flow rate, velocity, density, static temperature, pressure and area extension of the pseudo-source, respectively. As indicated, methane density at the pseudo-source is computed based on the ideal gas EoS. Further details are provided in the work of Birch et al. (1984).

Pseudo-source characteristic	**Equation**
Equivalent diameter	$d_{ps} = d\sqrt{C_D\left(\frac{p}{p_{amb}}\right)\left(\frac{2}{\gamma+1}\right)^{\frac{(\gamma+1)}{2(\gamma-1)}}}$
Mass flow rate	$\dot{m}_{ps} = \rho_{ps} \cdot A_{ps} \cdot v_{ps}$
Density	$\rho_{ps} = \frac{p_{ps} \cdot MW}{R \cdot T_{ps}}$
Pressure	$p_{ps} = p_{amb}$
Static temperature	$T_{ps} = T_{amb}$

Table 2: Boundary conditions used for all the simulations, detailing the specifics values assigned to each of them.

Boundary name	**Type**	**Specifics**
Back side	Velocity inlet	air, v_z = 5 m/s, T = 300 K
Top side	Velocity inlet	air, v_z = 5 m/s, T = 300 K
Left side	Velocity inlet	air, v_z = 5 m/s, T = 300 K
Ground	Wall	0.01 m roughness height, adiabatic
Symmetry	Symmetry	-
Front side	Pressure outlet	air, $T_{BACKFLOW}$ = 300 K
Nozzle	Wall	0.001 m roughness height, adiabatic
Methane jet	Mass flow inlet	Computed case by case according to Birch et al. (1984) model equations. See Table 1.
Spherical obstacle	Wall	0.001 m roughness height, adiabatic

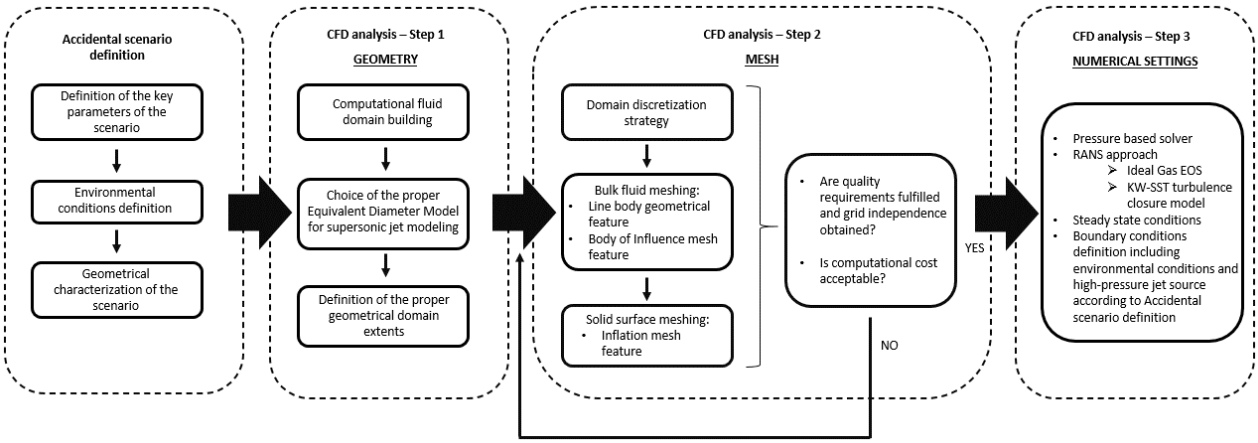

Fig. 3: Methodology flow chart.

3. RESULTS AND DISCUSSION

3.1 QUANTITATIVE RESULTS

The reliability of the present CFD modeling approach has been already demonstrated elsewhere (Colombini et al., 2020a), where the CFD results have been successfully compared to results derived from experimental campaigns on HP methane free jets. Therefore, it has not been further investigated in this work.

Prior to go through the results analysis, it has to be note that, to keep the focus of the work on the spherical obstacle influence, all the scenarios considered do not include any ground effect. Therefore, in Table 1S of the Supplemental information (which collects information and results related to all the scenarios considered in this work), the cases for which the ground interference was notified were not considered.

The first analysis performed was on the influence that legs (possibly coupled to a spherical obstacle to mime the usual spherical thanks configuration) have on the jet development. Considering run 10_M in Table 1S, Figure 4 clearly shows how the legs deviate toward the ground the jet cloud, considerably reducing its axial maximum extent (ME). This can be explained by comparing the flow fields of the two situations (see Figure 5): without legs, the flow field around the sphere is completely symmetric, while with legs the flow passing under the obstacle is disturbed, leading to a reduction of its velocity with respect to the flow on the top. As a consequence of this velocity imbalance, the flow is downward deviated.

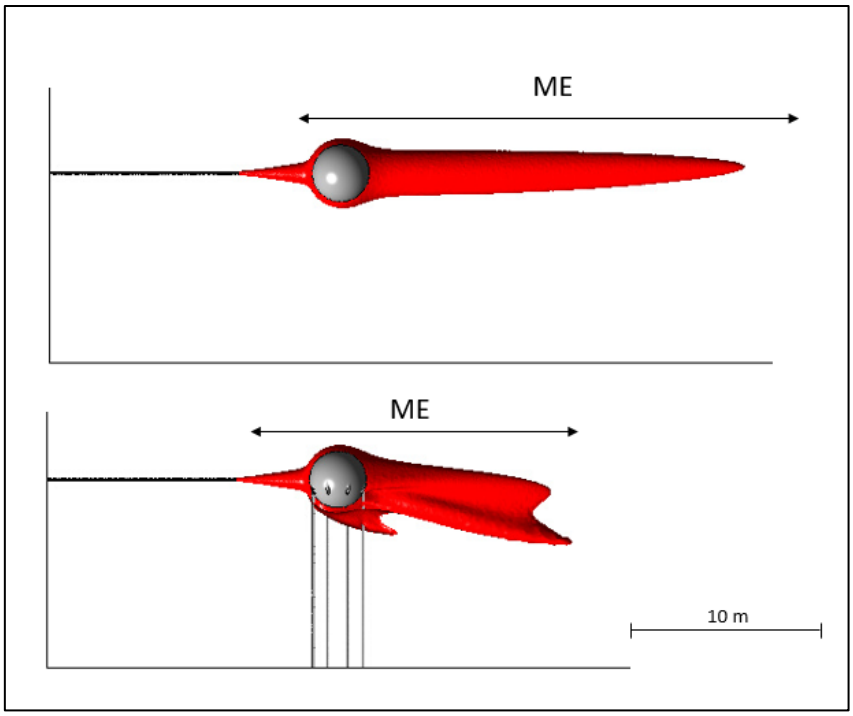

Fig. 4: Comparison of the jet clouds around the spherical obstacle with and without legs in terms of mole fraction isosurfaces (c = 5.3 %), highlighting the effect that legs have on the cloud shape development

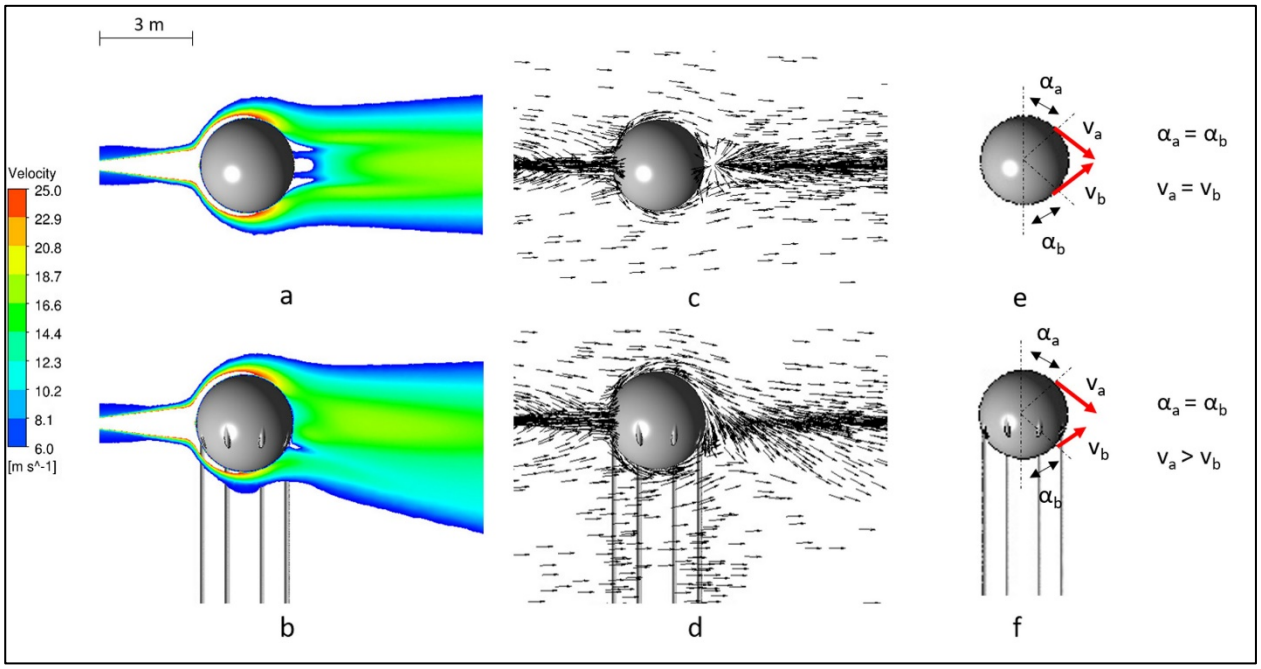

Fig. 5: Comparison of the flow field around the obstacles in terms of velocity contours (5a and 5b), and vectors plot along the vertical symmetry plane of the domain (5c and 5d). Fig. 5e and 5f schematize the

velocity field, highlighting the difference in their intensity (α is the angle between the vertical direction and the points in proximity of the solid surfaces where velocities are recorded).

To show how any of the scenario parameters introduced in Section 2 modifies the jet cloud development, Figure 6 reports the isosurfaces of some of the runs listed in Table 1S.

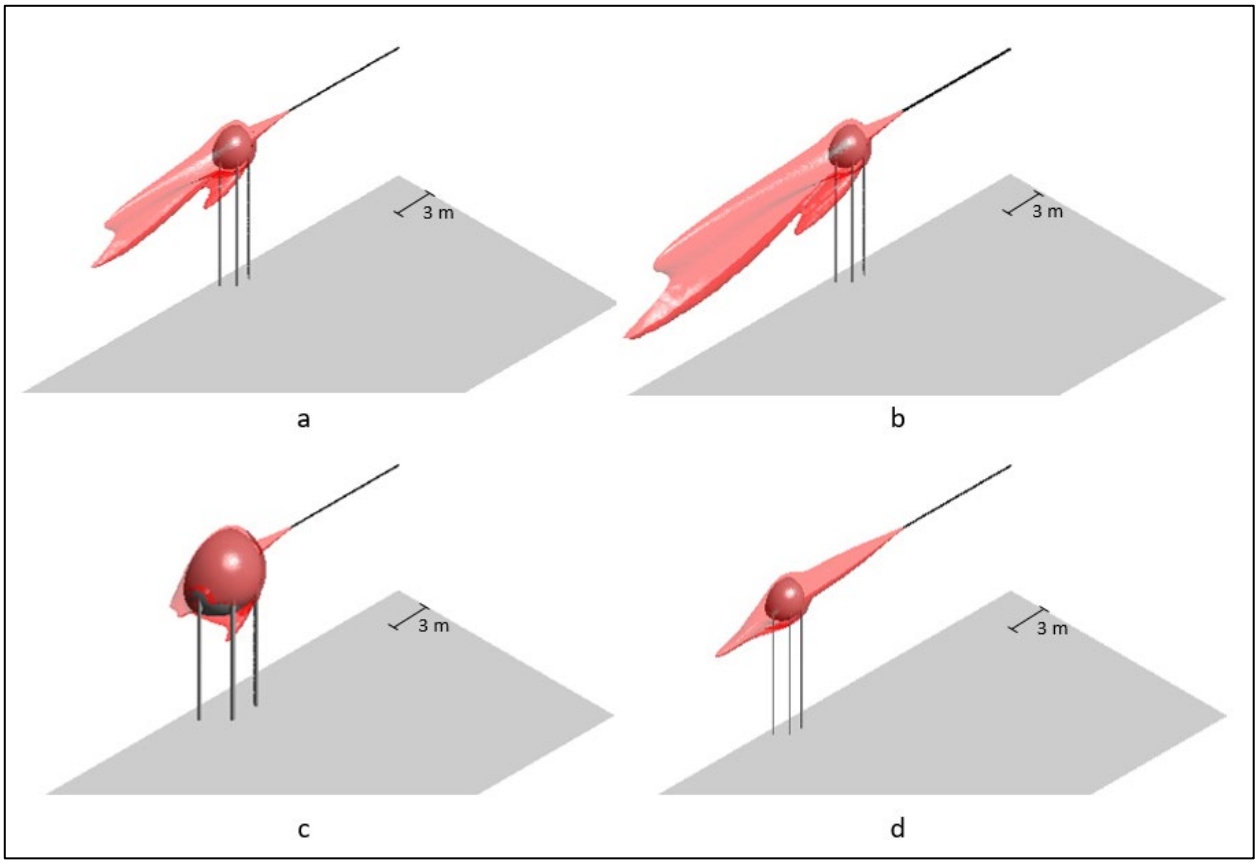

Fig. 6: Isosurfaces of the methane jet interacting with the spherical obstacle for some of the runs in Table 1S: (6a) run 10_M; (6b) run 50_M (greater upstream pressure); (6c) run 26_M (greater D_T); (6d) run 13_M (greater obstacle-jet source distance).

By way of example, considering run 10_M as reference case (Figure 6a), comparing the Figures shown we can say that, qualitatively: i) a greater upstream pressure (doubled) leads to a longer jet cloud (nearly 60 %) (Figure 6b, referred to run 50_M); ii) a greater obstacle diameter (doubled) leads to a shorter jet cloud that ends just over the obstacle (Figure 6c, referred to run 26_M); iii) a greater distance from the jet source (2.5 times) leads to a jet cloud practically of the same length of the one in the reference case (Figure 6d, referred to run 13_M). As a general observation, in all the cases shown in Figure 6 the jet cloud passes over the spherical obstacle. A more detailed analysis

of the effect that each of the scenario parameters has on the jet cloud development is provided in Section 4.

The results of the runs in Table 1S have been analysed with the help of the parameters sketched in Figure 7, namely: ME_{FJ}, which is the cloud ME computed for the correspondent free jet; and $d_{FJ}(D)$, which is the free jet diameter evaluated in correspondence of the spherical obstacle centre position. Note that both ME_{FJ} and $d_{FJ}(D)$ can be easily estimated using analytical correlations, as discussed elsewhere (Colombini et al., 2020c).

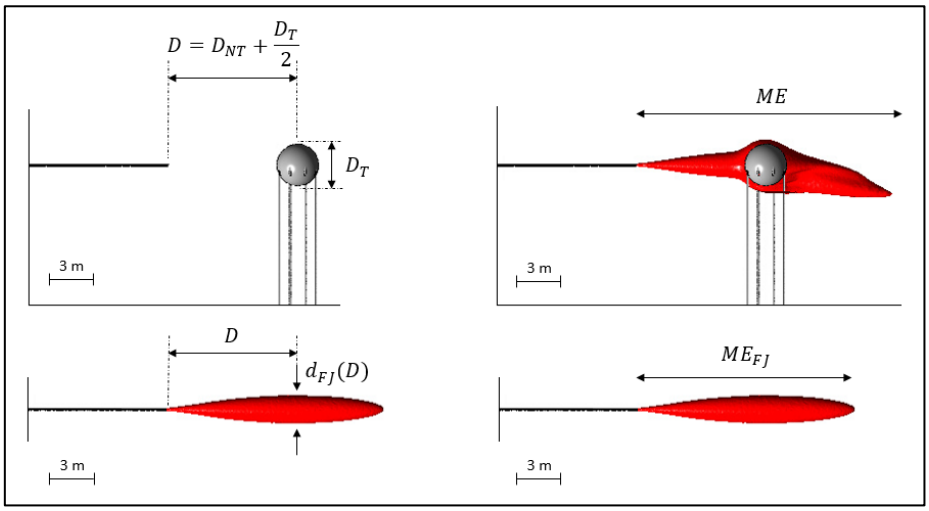

Fig. 7: Schematization of the parameters used to analyse the results obtained for runs in Table 1S, highlighting geometrical parameters and cloud parameters (both of impinging and free jet scenario).

These two parameters have been used to define two dimensionless parameters with the physical meaning of a ratio between two characteristic dimensions (one of the free jet, the other of the sphere: $d_{FJ}(D)/D_T$) and between two ME values (one of the jet impinging the sphere, the other of the free jet: ME/ME_{FJ}).

Figure 8 shows the results of the simulations carried out in terms of these two dimensionless parameters. From the Figure we can see a clear trend showing how the spherical obstacle influences the jet development:

- up to $d_{FJ}(D)/D_T \approx 0.5$, ME of the jet cloud is lower than (or equal to) the ME_{FJ} (considering a 10 % margin around $ME/ ME_{FJ} = 1$);
- for $d_{FJ}(D)/D_T$ comprised between about 0.5 and about 1, ME of the jet cloud linearly increases up to be 1.5 times greater than the ME_{FJ};

- over $d_{FJ}(D)/D_T \approx 1$, ME/ME_{FJ} of the jet cloud becomes almost constant (and approximately equal to 1.5).

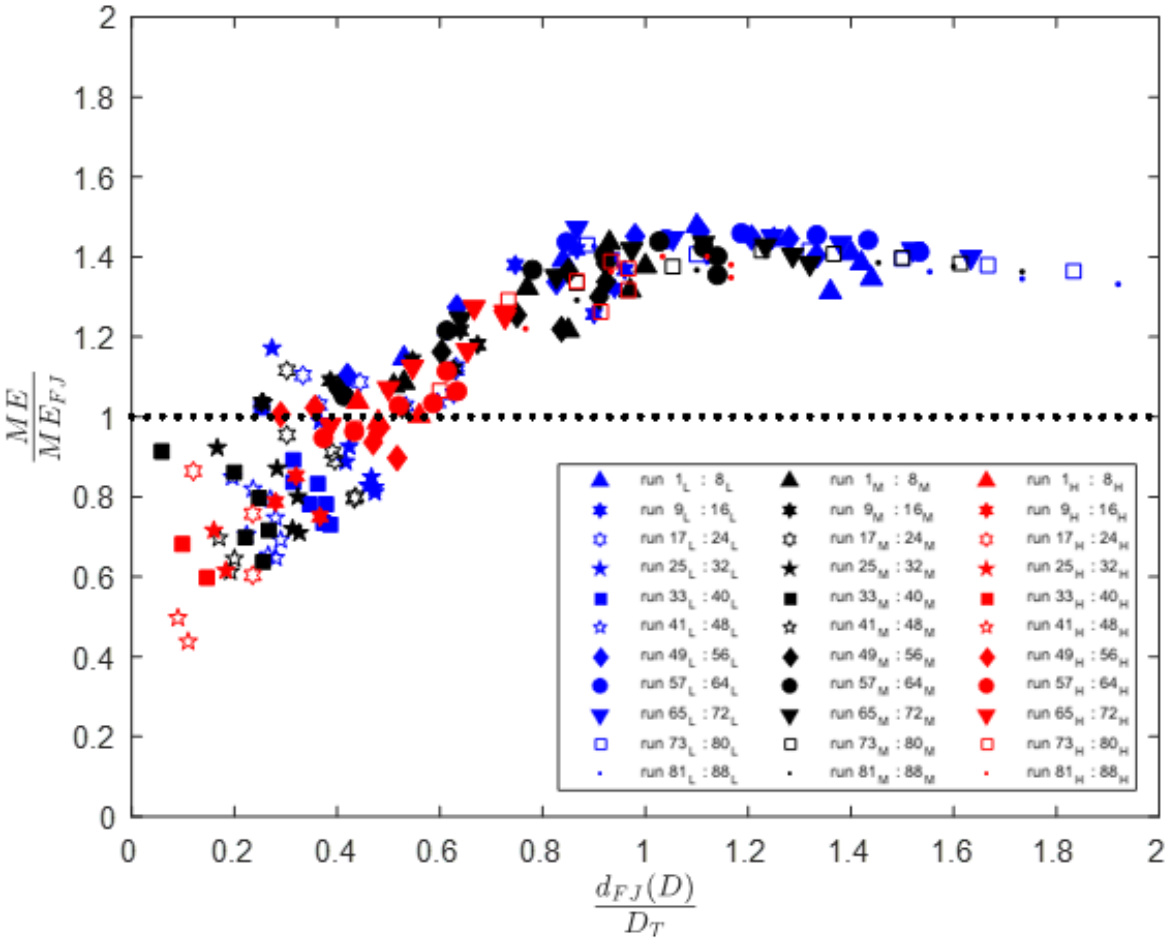

Fig. 8: Results of runs in Table 1S. Markers' colour defines the methane concentration level observed: blue is for the low level (c = 3.5 %), red is for the mean level (c = 5.3 %) and black is for the high level (c = 10 %). In the Figure, the dotted line identifies when the jet cloud ME is equal to the ME of the correspondent free jet. Markers' shape meaning is as reported in Figure legend.

Therefore, independently on the scenario specifics, the spherical obstacle induces two main effects:

- when the obstacle diameter is, at least, two times the free jet width (evaluated in correspondence of the obstacle centre position), the obstacle acts more like a wall and it reduces the cloud ME with respect to the correspondent free jet, leading to a safer situation;
- when the free jet width (evaluated in correspondence of the obstacle centre position) is, at least, half of the obstacle diameter, the jet cloud ME results to be increased with respect to

the correspondent free jet, leading to a less safe situation; in the worst case, the ME of the free jet is almost 1.5 times increased by the presence of the obstacle.

This can be summarized in the following conservative relations to estimate the ME of methane jet impinging a spherical obstacle:

$$\begin{cases} ME \sim ME_{FJ} & if \quad \dfrac{d_{FJ}(D)}{D_T} < 0.5 \\ ME \sim 1.5 \cdot ME_{FJ} & if \quad \dfrac{d_{FJ}(D)}{D_T} \geq 0.5 \end{cases}$$

3.2 QUALITATIVE RESULTS

This Section provides an analysis highlighting, by a general point of view, what is the qualitative effect on the jet cloud development when some characteristic parameters of a jet impacting a spherical obstacle are alternatively varied. These parameters are both some of the ones defined in Section 2 (*i.e.*, p, D_T, and c) and others not previously considered, such as the number of legs and the legs diameter.

An increase of the upstream pressure value leads to an increase of the mass flow rate, resulting in a larger jet cloud, as shown in Figure 9 for four runs of Table 1S (namely, run 12_M, 52_M, 68_M and 84_M). As expected from the results summarized in Figure 7, since in these cases $d_{FJ}(D)/D_T$ is always larger than 0.5 we found that the ratio ME/ME_{FJ} is always greater than one and equal to about 1.2-1.3.

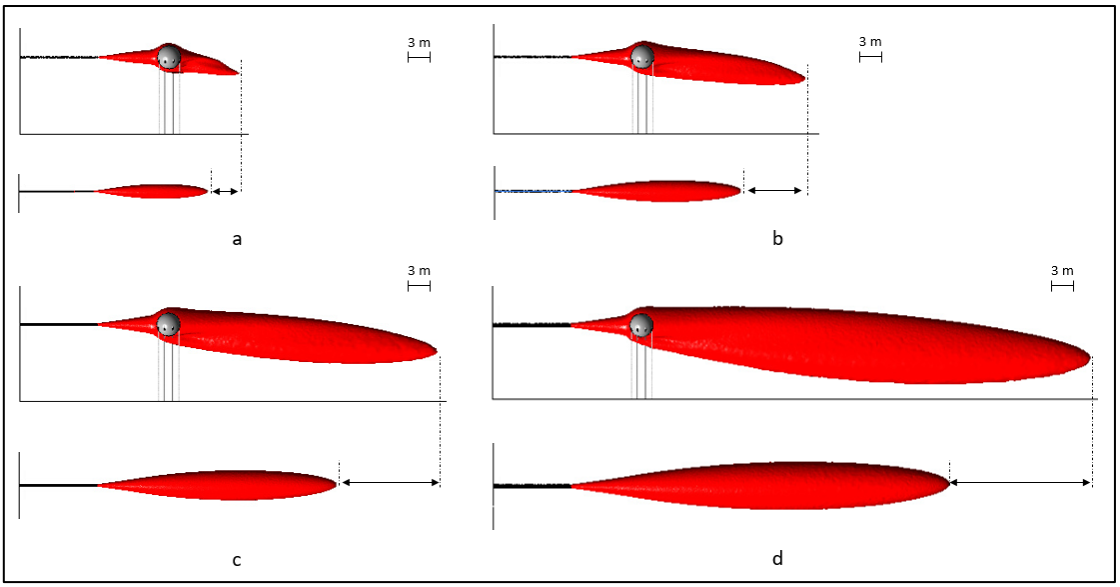

Considering a variation of the obstacle diameter, the larger D_T is, the more the jet path is obstructed by the obstacle. Therefore, it can be expected that an increase of D_T will result in a decrease of the jet cloud extent. In fact, the isosurfaces of methane concentration in air (c = 5.3 %) compared in Figure 10 for four selected runs of Table 1S (namely, run 9_M, 17_M, 25_M and 33_M) confirm what foreseen. About D_T variation, it is also interesting to note that the larger the D_T is, the more the deviation of the jet cloud toward the ground is, downstream the obstacle. The reason can be explained by looking at the flow field around the spherical obstacles. The larger the D_T is, the more the velocity intensity of the jet is reduced downstream the obstacle. Coupling this effect with the legs one (*i.e.,* that generates a velocity imbalance between the flows passing immediately above and below the obstacle), it leads to a predominance of the flow coming from the top side, resulting in a more downward deflection of the downstream flow field (see Figure 11).

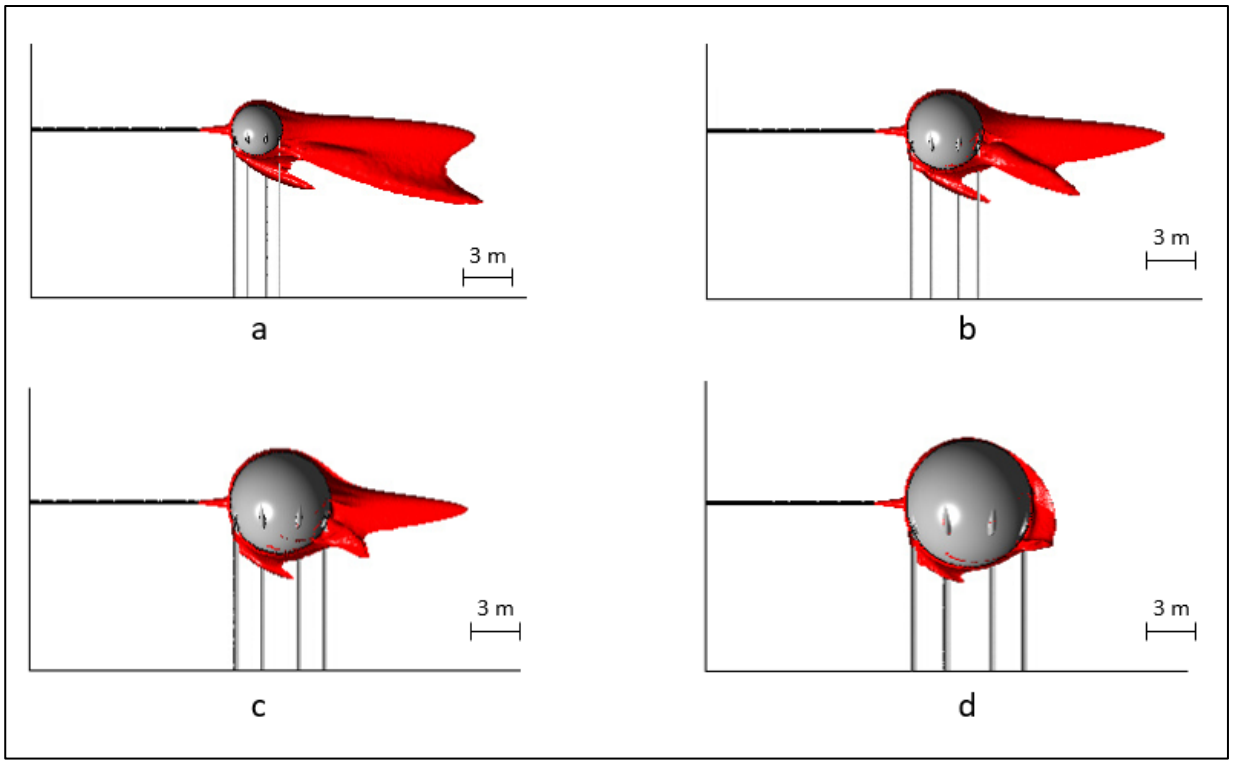

Sensitivity analysis on the effect that a variation of D_T (diameter of the spherical obstacle) has on the jet cloud development. Results are in terms of isosurfaces of methane concentration in air equal to 5.3%, when same jet source and same distance of the obstacle surface from the jet source are considered. (10a) D_T = 3 m (run 9_M); (10b) D_T = 4.5 m (run 17_M); (10c) D_T = 6 m (run 25_M); (10d) D_T = 7.5 m (run 33_M).

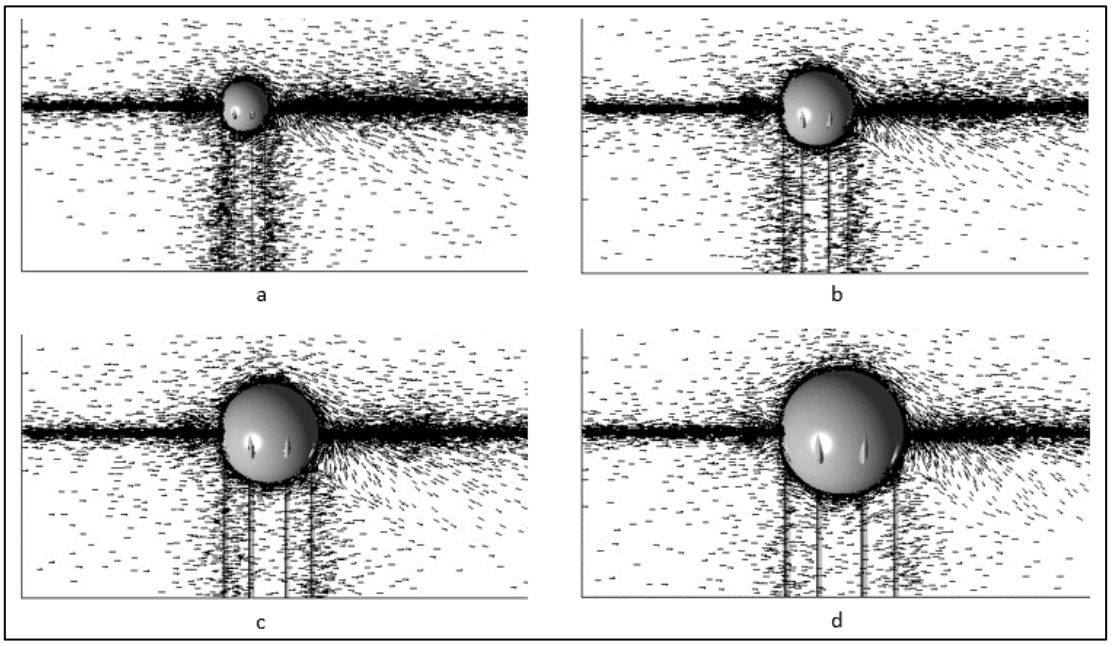

Sensitivity analysis on the effect that the variation of D_T (diameter of the spherical obstacle) has on the jet cloud development. Results are in terms of flow field vectors plot when same jet source and same

distance of the obstacle surface from the jet source are considered. (11a) D_T = 3 m (run 9_M); (11b) D_T = 4.5 m (run 17_M); (11c) D_T = 6 m (run 25_M); (11d) D_T = 7.5 m (run 33_M).

Lowering the observed concentration of methane in air leads to increase the cloud size. Therefore, as expected from the results summarized in Figure 8, the greater the size of the jet cloud is, the larger the obstacle influence on the cloud development is expected to be. Considering run 12_M of Table 1S, Figure 12 shows that the lower the concentration level observed is, the more the influence of the spherical obstacle on the jet cloud results to be.

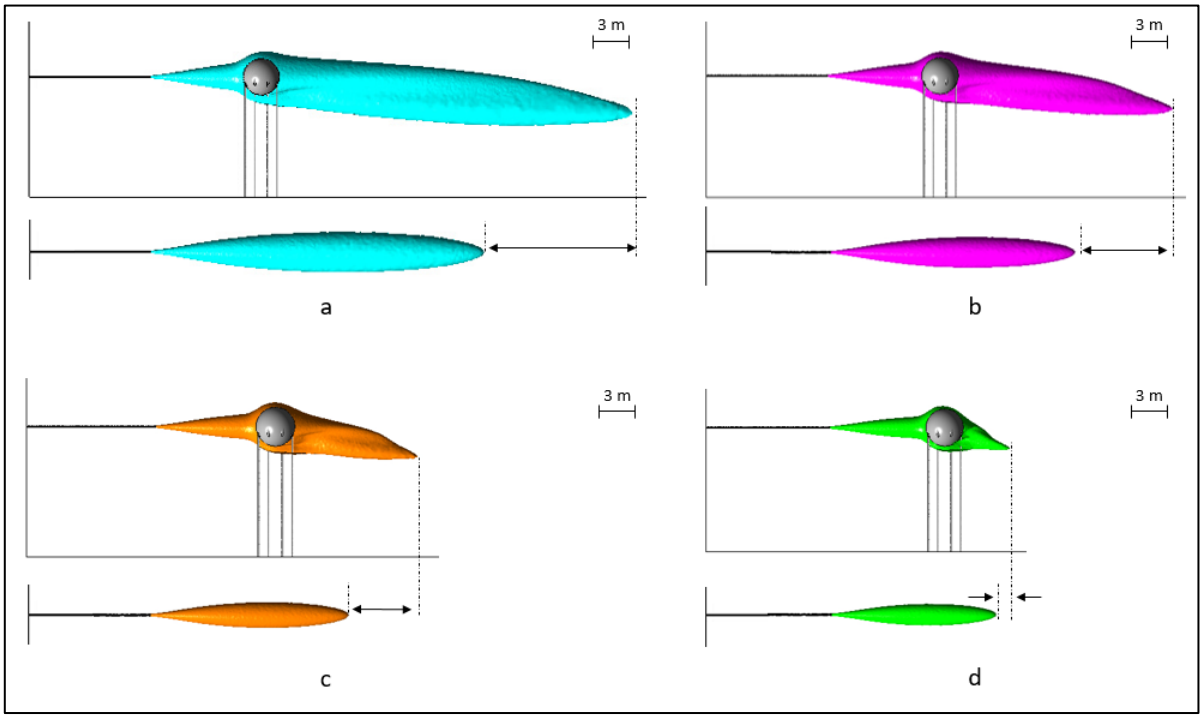

Fig. 12: Sensitivity analysis on the effect that a variation of observed methane concentration has on the jet cloud development (both for impinging and free jet scenario). Results are in terms of isosurfaces of methane concentration in air equal to: 3% (12a); 4% (12b); 5% (12c); and 6% (12d).

Focusing on how the jet cloud may be modified only by obstacle legs characteristics, two analysis varying alternatively the number of legs and their diameter were performed. Starting from what observed in Section 3, we can say that the more the number and diameter of the legs are, the more the interference on the flow field will be expected to be enhanced. Therefore, a shorter and more downward directed jet cloud would be expected for larger values of D_L or N_L. Considering run 9_M of Table 1S as benchmark case (Figure 13a), Figure 13b (where D_L was varied) and 13c

(where N_L was varied) confirm such legs-related effect. As we can see, both an increase of N_L (Figure 13a with respect to Figure 13c) and D_L (Figure 13b with respect to Figure 13a) leads to a ME reduction together with a cloud more oriented towards the ground. From the Figures, it is noticeable that, with respect to a reasonable variation of the two legs characteristics within a realistic range (namely, new N_L = 4 while new D_L = 0.353 m), the variation of N_L largely affects the jet cloud development with respect to what a similar variation of D_L does.

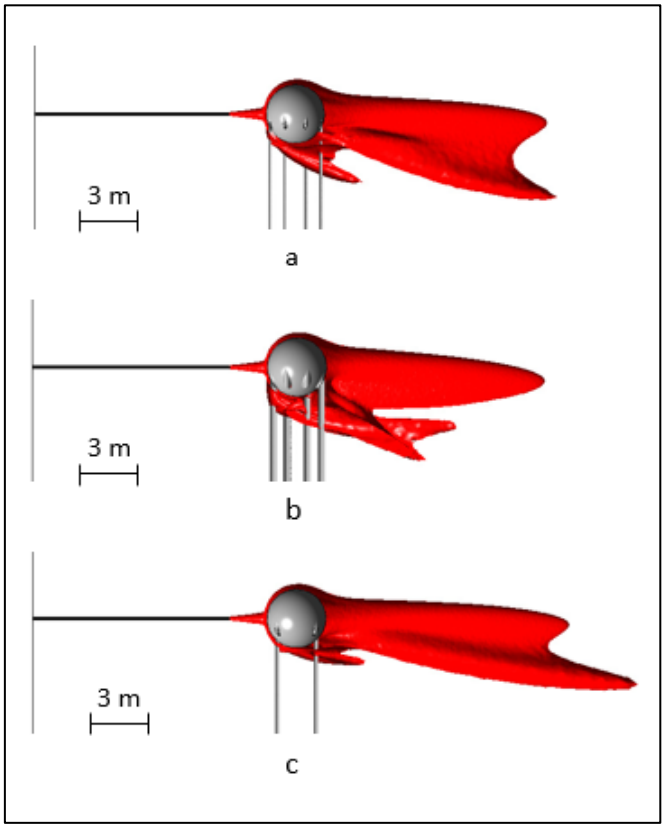

Fig. 13 Sensitivity analysis on the effect that a variation of legs number (N_L) or legs diameter (D_L) has on the jet cloud development. (13a) run 9_M; (13b) double legs diameter; (13c) half the legs number. Results are in terms of isosurfaces of methane concentration in air equal to 5.3 %.

3.3 DISCUSSION

As outcome of the work performed, analyzing the effect that a spherical obstacle may have on the cloud development and consequent area involvement of an accidental high-pressure methane release, the following rule of thumb to estimate the influence on the ME of the impinging jet was derived:

1. From the source characteristics, estimate the ME_{FJ} value using the Chen and Rodi (1980) concentration decay model, whose model reliability in estimating ME_{FJ} is discussed elsewhere (Colombini et al., 2020a):

$$ME_{FJ} = \frac{k d_{ps}}{\bar{c}} \left(\frac{\rho_{amb}}{\rho_{ps}} \right)^{\frac{1}{2}}$$

Here $\bar{c}$ is the specific methane concentration in air considered, k is the axial decay constant (equal to 4.4, as suggested by Birch et al., 1984), d_{ps} is the pseudo-source orifice diameter (computed with the model of Birch et al., 1984: see Table 1), ρ_{amb} is the air density, and ρ_{ps} is the methane density at pseudo-source conditions.

2. From the source characteristics, estimate $d_{FJ}(D)$ as (Cushman-Roisin, 2020; Chen and Rodi, 1980):

$$d_{FJ}(D) = 2 \cdot \sqrt{-\frac{D^2}{50} \cdot \ln\left(\frac{\bar{c}}{c_{ax}(D)} \right)}$$

where

$$c_{ax}(D) = \frac{k d_{ps}}{D} \left(\frac{\rho_{amb}}{\rho_{ps}} \right)^{\frac{1}{2}}$$

where D is the distance of the spherical obstacle centre from the jet source, $c_{ax}(D)$ is the methane concentration along the free jet axis computed in correspondence of the spherical obstacle centre position. Also, the Cushman-Roisin (2020) model reliability in estimating $d_{FJ}(D)$ is discussed in detail elsewhere (Colombini et al., 2020c).

3. If $d_{FJ}(D) / D_T < 0.5$, ME_{FJ} provides a conservative order of magnitude of ME
4. If $d_{FJ}(D) / D_T \geq 0.5$, a conservative order of magnitude of ME can be estimated as $1.5 \cdot ME_{FJ}$

The four steps procedure detailed rely on knowing information of the scenario under investigation (i.e., obstacle geometry and source characteristics) and consolidated literature models. It can be used as alternative for consequence calculation step within QRA analysis, when a spherical obstacle is concerned. In particular, it is possible to evaluate, by order of magnitude, how it will be the extent of a flash fire event. Obviously, it should be stressed that this procedure is expected to provide a reasonable, and almost always conservative by the industrial safety point of view, estimation as an order of magnitude of ME only inside the parameter window investigated (*i.e.*,

for methane only, for upstream pressures between 65 and 650 bar, for upstream temperature equal to 278 K, for orifice diameter equal to 0.0254 m, for spherical obstacle diameters between 2 and 10 m, for distances of the obstacle from the source between 25 and 100 % of the free jet length and for methane concentration levels observed between 3.5 and 10 %). Among the others, the effect of the presence of more than one obstacle, as well as that of an obstacle together with the ground, were not investigated and they deserve further investigations. Therefore, the use of detailed CFD simulations should be considered, both for confirming the estimated values and for obtaining more reliable estimations.

5. CONCLUSIONS

As a matter of fact, the methane high-pressure gaseous release is a relevant safety-related problem mainly in the Oil and Gas (O&G) industry. In this work, the scenario of a spherical obstacle impinged by a methane HP jet was investigated through a CFD-based model. The analysis showed that the spherical obstacle either decreases or increases the ME of the jet cloud with respect to the free jet. As main outcome of practical importance, this work provides a brief by-hand procedure that, only based on known scenario information (or information that can be recovered by applying analytical literature models), allows estimating the maximum extent of the unignited high-pressure jet when interacting with a spherical obstacle. Within the limitations previously discussed, this procedure can be used as an order of magnitude estimation for a first attempt consequence calculation within QRA analysis.

COMPETING INTERESTS STATEMENT

The Authors declare that there is no conflict of interest.

ACKNOWLEDGEMENTS

This research did not receive any specific grant from funding agencies in the public, commercial, or not-for-profit sectors.

REFERENCES

Angers, B., Hourri, A., Benard, P., Tchouvelev, A., 2011. Numerical investigation of a vertical surface on the flammable extent of hydrogen and methane vertical jets. *Int. J. Hydrogen Energy* 36, 2567-72.

Ansys DesignModeler User's Guide, 2017. Release 19.0. ANSYS, Inc.

Ansys Fluent User's Guide, 2017. Release 19.0. ANSYS, Inc.

Ansys Meshing User's Guide, 2017. Release 19.0. ANSYS, Inc.

Ansys Workbench User's Guide, 2017. Release 19.0. ANSYS, Inc.

Becker, H.A., Hottel, H.C., williams, G.C., 1967. The nozzle-fluid concentration of the round, turbulent free jet. *J. Fluid Mech.* 30, 285-303. https://doi.org/10.1017/S0022112067001430

Bénard, P., Tchouvelev, A., Hourri, A., Chen, Z., Angers, B., 2007. High pressure hydrogen jets in the presence of a surface. *Int. Conf. Hydrog. Saf.* 40.

Bénard, P., Hourri, A., Angers, B., Tchouvelev, A., Agranat, V., 2009. Effects of surface on the flammable extent of hydrogen jets. *Int. Conf. Hydrog. Saf*.

Bénard, P., Hourri, A., Angers, B., Tchouvelev, A., 2016. Adjacent surface effect on the flammable cloud of hydrogen and methane jets: Numerical investigation and engineering correlations. *Int. J. Hydrogen Energy* 41, 18654–18662. https://doi.org/10.1016/j.ijhydene.2016.08.173.

Bernatik, A., Libisova, M., 2004. Loss prevention in heavy industry: Risk assessment of large gasholders. *J. Loss Prev. Process Ind.* 17(4), 271.

Birch, A.D., Brown, D.R., Dodson, M.G., Swaffield, F., 1984. The structure and concentration decay of high pressure jets of natural gas. *Combust. Sci. Technol.* 36, 249–261. https://doi.org/10.1080/00102208408923739.

Brook, D. R., Felton, N. V., Clem, C. M., Strickland, D. C. H., Griffiths, I. H., Kingdon, R. D., 2003. Validation of the urban dispersion model (UDM). *Int. J. Environ. Pollut.* 20 (1−6), 11.

Cameron, I., Raman, R., 2005. Process System Risk Management, first ed. Elsevier Amsterdam.

Chen, C.J., Rodi, W., 1980. Vertical Turbulent Buoyant Jets – A review of Experimental Data, First ed. Pergamon Press Vol. 4.

Colombini, C., Busini, V., 2019a. Obstacle Influence on High-Pressure Jets based on Computational Fluid Dynamics Simulations. *Chem. Eng. Trans.* 77, 811–816. https://doi.org/10.3303/CET1977136.

Colombini, C., Busini, V., 2019b. High-Pressure Methane Jet: Analysis of the Jet-Obstcle Interaction. *Proceeding of the 29th European Safety and Reliability Conference.*

Colombini, C., Martani, A., Rota, R., Busini, V., 2020a. Ground influence on high-pressure methane jets: Practical tools for risk assessment. *J. Loss Prevent. Proc.* 67, 104240. https://doi.org/10.1016/j.jlp.2020.104240

Colombini, C., Carlini, L., Rota, R., Busini, V., 2020b. Ground Interaction on High-Pressure Jets: Effect on Different Substances. *Chem. Eng. Trans.* 82. https://doi.org/10.3303/CET2082062

Colombini, C., Maugeri G., Zanon, G., Rota, R., Busini, V., 2021. Unignited High-Pressure Methane Jet Impinging a Pipe Rack: Practical Tools for Risk Assessment. *J. Loss Prevent. Proc. 69, 104378* https://doi.org/10.1016/j.jlp.2020.104378

Cushman-Roisin, B., Environmental Fluid Mechanics – John Wiley & Sons, Book in preparation. Last online access: August 2020. http://www.dartmouth.edu/~cushman/books/EFM/chap9.pdf

Dasgotra, A., Varun Teja, G. V.V., Sharma, A., Mishra, K.B., 2018. CFD modeling of large-scale flammable cloud dispersion using FLACS. *J. Loss Prev. Process Ind.* 56, 531–536. https://doi.org/10.1016/j.jlp.2018.01.001.

Deng, Y., Hu, H., Yu, B., Sun, D., Hou, L., Liang, Y., 2018. A method for simulating the release of natural gas from the rupture of high-pressure pipelines in any terrain. *J. Hazard. Mater.* 342, 418–428. https://doi.org/10.1016/j.jhazmat.2017.08.053.

Derudi, M., Bovolenta, D., Busini, V., Rota, R., 2014. Heavy gas dispersion in presence of large obstacles: Selection of modeling tools. *Ind. Eng. Chem. Res.* 53, 9303–9310. https://doi.org/10.1021/ie4034895.

Desilets, S., Cote, S., Nadau, G., Benard, P., Tchouvelev, A., 2009. Experimental results and comparison with simulated data of a low pressure hydrogen jet. *Int. Conf. Hydrog. Saf*.

Dey, S., Kishore, G.R., Castro-Orgaz, O., Ali, S.Z., 2017. Hydrodynamics of submerged turbulent plane offset jets. *Phys. Fluids* 29. https://doi.org/10.1063/1.4989559.

Efthimiou, G.C., Andronopoulos, S., Tavares, R., Bartzis, J.G., 2017. CFD-RANS prediction of the dispersion of a hazardous airborne material released during a real accident in an industrial environment. *J. Loss Prev. Process Ind.* 46, 23–36. https://doi.org/10.1016/j.jlp.2017.01.015.

EPA, 2011. Computer-Aided management of emergency operations (CAMEO), ALOHA v.5.4.1, http://epa.gov/ceppo/cameo/aloha.htm

Franquet, E., Perrier, V., Gibout, S., Bruel, P., 2015. Free underexpanded jets in a quiescent medium: A review. *Prog. Aerosp. Sci.* 77, 25–53. https://doi.org/10.1016/j.paerosci.2015.06.006.

Gerbec, M., Pontiggia, M., Antonioni, G., Tugnoli, a., Cozzani, V., Sbaouni, M., Lelong, R., 2017. Comparison of UDM and CFD simulations of a time varying release of LPG in geometrical

complex environment. *J. Loss Prev. Process Ind.* 45, 56–68. https://doi.org/10.1016/j.jlp.2016.11.020.

Hall, J.E., Hooker, P., O'Sullivan, L., Angers, B., Hourri, A., Benard, P., 2017. Flammability profiles associated with high-pressure hydrogen jets released in close proximity to surfaces. *Int. J. Hydrogen Energy* 42, 7413–7421. https://doi.org/10.1016/j.ijhydene.2016.05.113.

Hess, K., Leukel, W., Stoeckel, A., 1973. Formation of explosive clouds on overhead release and preventive measure. *Chemie-Ingenieur-Technik* 45, 5.

Houf, W., Schefer, R., Evans, G., Merilo, E., Groethe, M., 2010. Evaluation of barrier walls for mitigation of unintended releases of hydrogen. *Int. J. Hydrogen Energy* 35, 4758–4775. https://doi.org/10.1016/j.ijhydene.2010.02.086.

Hourri, A., Angers, B., Bénard, P., 2009. Surface effects on flammable extent of hydrogen and methane jets. *Int. J. Hydrogen Energy* 34, 1569–1577. https://doi.org/10.1016/j.ijhydene.2008.11.088.

Hourri, A., Angers, B., Bénard, P., Tchouvelev, A., Agranat, V., 2011. Numerical investigation of the flammable extent of semi-confined hydrogen and methane jets. *Int. J. Hydrogen Energy* 36, 2567–2572. https://doi.org/10.1016/j.ijhydene.2010.04.121.

Hu, J., Christopher, D.M., Li, X., 2018. Simplified partitioning model to simulate high pressure under-expanded jet flows impinging vertical obstacles. *Int. J. Hydrogen Energ*. 43, 13649-13658. https://doi.org/10.1016/j.ijhydene.2018.05.036

Jafari, M., Mohammadfam, I., Zarei, I., 2014. Analysis and Simulation of Severe Accidents in a Steam Methane Reforming Plant. *Int. J. Occup. Hyg.* 6, 120-130.

Jhonston, I.A., 2005. The Noble-Abel Equation of State: Thermodynamic Derivations for Ballistics Modelling. *Weapons Systems Division Defence Science and Technology Organisation*. DSTO-TN-0670.

Jiang, Y., Xu, Z., Wei, J., Teng, G., 2020. Fused CFD-interpolation model for real-time prediction of hazardous gas dispersion in emergency rescue. *J. Loss Prev. Process Ind.* 63, 103988. https://doi.org/10.1016/j.jlp.2019.103988.

Luo, T., Yu, C., Liu, R., Li, M., Zhang, J., Qu, S., 2018. Numerical simulation of LNG release and dispersion using a multiphase CFD model. *J. Loss Prev. Process Ind.* 56, 316–327. https://doi.org/10.1016/j.jlp.2018.08.001.

Menter, F.R., 1993. Zonal Two Equation kω Turbulence Models for Aerodynamic Flows. *24th Fluid Dynamics Conference*.

Middha, P., Hansen, O.R., Grune, J., Kotchourko, A., 2010. CFD calculations of gas leak dispersion and subsequent gas explosions: Validation against ignited impinging hydrogen jet experiments. *J. Hazard. Mater.* 179, 84–94. https://doi.org/10.1016/j.jhazmat.2010.02.061.

Pandya, N., Gabas, N., Marsden, E., 2012. Sensitivity analysis of Phast's atmospheric dispersion model for three toxic materials (nitric oxide, ammonia, chlorine). *J. Loss Prev. Process Ind.* 25 (1), 20.

Pontiggia, M., Busini, V., Ronzoni, M., Uguccioni, G., Rota, R., 2014. Effect of large obstacles on high momentum jets dispersion. *Chem. Eng. Trans.* 36, 523–528. https://doi.org/10.1016/j.jhazmat.2009.06.064.

Rian, K., Evanger, T., Vembe, B., Lilleheie, N., Lakså, B., Hjertager, B., Magnussen, B., 2016. Coherent computational analysis of large-scale explosions and fires in complex geometries – from combustion science to a safer oil and gas industry. *Chem. Eng. Trans* 48, 175-180 https://doi.org/10.3303/CET1648030

Schleder, A.M., Pastor, E., Planas, E., Martins, M.R., 2015. Experimental data and CFD performance for cloud dispersion analysis: The USP-UPC project. *J. Loss Prev. Process Ind.* 38, 125-138.

Souza, A. O., Luiz, A. M., Neto A. T. P., Araujo A. C. B., Silva H. B., Silva A. K., Alves J. J. N, 2019a. A new correlation for hazardous area classification based on experiments and CFD predictions. *Process Saf. Prog.* 38, 21–26. https://doi.org/10.1002/prs.11974.

Souza, A. O., Luiz, A. M., Neto A. T. P., Araujo A. C. B., Silva H. B., Silva A. K., Alves J. J. N, 2019b. CFD predictions for hazardous area classification. *Chinese J. Chem. Eng.* 27, 21–31. https://doi.org/10.1016/j.cjche.2018.06.002

Sposato, C., Tamanini, F., Rogers, W.J., Sam Mannan, M., 2003. Effects of Plate Impingement on the Flammable Volume of Fuel Jet Releases. *Process Saf. Prog.* 22, 4. https://doi.org/10.1002/prs.680220406

Stewart, J.R., 2019. CFD modelling of underexpanded hydrogen jets exiting rectangular shaped openings. *Inst. Chem. Eng. Symp. Ser.* 2019-May.

Sun, Z.-Y., 2019. Experimental studies on the explosion indices in turbulent stoichiometric H2/CH4/air mixtures. *Int. j. hydrogen energ.* 44, 469-476 https://doi.org/10.1016/j.ijhydene.2018.02.094

Tchouvelev, A.V., Cheng, Z., Agranat, V.M., Zhubrin, S.V., 2007. Effectiveness of small barriers as means to reduce clearance distances. *Int. J. Hydrogen Energy* 32, 1409–1415. https://doi.org/10.1016/j.ijhydene.2006.10.020.

Thring, M.W.,Newby, M.P., Combusiton length of enclosed turbulent jet flames, 1952. 4th International symposium on combusiton, 789, williams and Wilkins, Pittsburgh, PA.

Tolias, I. C., Giannissi, S.G., Venetsanos, A.G., Keenan, J., Shentsov, V., Makarov, D., Coldrick, S., Kotchourko, A., Ren, K., Jedicke, O., Melideo, D., Baraldi, D., Slater, S., Duclos, A., Verbecke, F., Molkov, V., 2019. Best practice guidelines in numerical simulations and CFD benchmarking for hydrogen safety applications. *Int. J. Hydrogen Energy* 44, 9050–9062. https://doi.org/10.1016/j.ijhydene.2018.06.005.

Uggenti, A.C., Carpignano, A., Savoldi, L., Zanino, R., 2017. Perspective and criticalities of CFD modelling for the analysis of oil and gas offshore accident scenarios. *Risk, Reliability and Safety: Innovating Theory and Practice: Proceedings of ESREL 2016.*

Varsegova, E., Dresvyannikova, E., Osipova, L., Sadykov, R., 2019. Damage areas during emergency depressurization of a gas pipeline. *EECE Proceedings.* 140, 06007. https://doi.org/10.1051/e3sconf/201914006007

Wilkening, H., Baraldi, D., 2007. CFD modelling of accidental hydrogen release from pipelines, *Int. J. Hydrogen Energ.,* Volume 32 (13), 2206-2215. https://doi.org/10.1016/j.ijhydene.2007.04.022

Zhang, Y., Zhu, J., Teng, L., Song, C., 2020. Experimental research of LNG accidental underwater release and combustion behavior. *J. Loss Prevent. Proc.* 64, 104036. https://doi.org/10.1016/j.jlp.2019.104036

Zhou, K., Wang, X., Liu, M., Liu, J., 2018. A theoretical framework for calculating full-scale jet fires induced by high-pressure hydrogen/natural gas transient leakage. *Int. j. hydrogen energ.* 43, 22765-775. https://doi.org/10.1016/j.ijhydene.2018.10.122

Zhu, H., Mao, Z., Wang, Q., Sun, J., 2013. The influences of key factors on the consequences following the natural gas leakage from pipeline. *Procedia Engineer.* 62, 592-601. https://doi.org/10.1016/j.proeng.2013.08.104

Zhu, Y., Wang, D., Shao, Z., Zhu, X., Xu, C., Zhang, Y., 2020. Investigation on the overpressure of methane-air mixture gas explosions in straight large-scale tunnels. *Process Saf. Environ.* 135, 101-112. https://doi.org/10.1016/j.psep.2019.12.022

Zuliani, C., De Lorenzi, C., Ditali, S., 2016. Application of CFD Simulation to Safety Problems – Challenges and Experience Including a Comparative Analysis of Hot Plume Dispersion from a Ground Flare. *Chem.Eng. Trans.* 53, 79-84. https://doi.org/10.3303/CET1653014